J Mater Sci (2007) 42:1577–1583
DOI 10.1007/s10853-006-0988-5

Characterization of nanostructured metals produced by plastic deformation

Xiaoxu Huang

Received: 28 June 2006 / Accepted: 21 September 2006 / Published online: 16 December 2006

Abstract Nanostructured metals produced by plastic deformation often exhibit characteristic structural features such as elongated morphology, a bimodal misorientation distribution and the presence of interior dislocations. The characterization of these parameters is demonstrated by results of TEM and EBSD analyses of pure Ni processed by high pressure torsion (HPT) and pure Al processed by accumulative roll bonding (ARB). Care needed in selecting sample plane and characterization technique is discussed.

Introduction

Nanostructured metals can be produced by deformation to extremely high strains (severe plastic deformation) [1, 2], electrodeposition [3] or by the compaction of nanometre-sized metal powders [4]. The nanostructured metals produced by these techniques are different from a recrystallized metal and a precise characterization of the structural parameters is thus essential for understanding the mechanical and thermal behavior of these fine-scaled metals. Various techniques, such as transmission electron microscopy (TEM), high resolution TEM (HRTEM), electron backscatter diffraction (EBSD) in a scanning electron microscope (SEM) and X-ray diffraction (XRD), can be used in these structural studies (Table 1). However, care is required in selecting the characterization techniques and in interpreting the results obtained. For example, Mitra et al. [5] made a comparison of grain size measurements by XRD and TEM methods for bulk nanocrystalline copper processed by inert gas condensation and compaction. They found that the TEM results agree well with those of XRD measurements for a narrow grain size distribution with small mean values, but they deviated significantly when the grain size increased and distributions widened, indicating that the information from XRD analysis could be misleading. Recently, Rentenberger et al. [6] made an excellent review of HRTEM analysis of nanostructured alloys produced by severe plastic deformation. They pointed out several issues related to the Moiré effect that may cause misinterpretation of the TEM image contrast and boundary structure and lead to errors when calculating the dislocation density within the structure.

This paper focuses on TEM and EBSD characterization of nanostructured metals produced by plastic deformation. Results obtained from pure Ni processed by high pressure torsion (HPT) and pure Al processed by accumulative roll bonding (ARB) are taken as examples to demonstrate the characteristic structural parameters including structural morphology, boundary spacing, boundary misorientation and interior dislocation density. In particular, the importance of selecting a proper sample plane and characterization technique is discussed.

X. Huang (✉)
Center for Fundamental Research: Metal Structures in Four Dimensions, Materials Research Department, Risø National Laboratory, DK-4000 Roskilde, Denmark
e-mail: xiaoxu.huang@risoe.dk

Structural morphology

Deformation-produced nanostructures exhibit typically an elongated (a lamellar) or an equiaxed appearance.

Table 1 Structural parameters and characterization techniques

Structural parameter	Technique
Morphology	TEM, HRTEM, EBSD/SEM
Spacing (size)	TEM, HRTEM, EBSD/SEM, XRD
Misorientation	TEM, HRTEM, EBSD/SEM
Dislocation density	TEM, HRTEM, XRD

The elongated structure is often observed in nanostructures produced by monotonic deformation, such as cold rolling [7], ARB [8] and HPT [9]. An equiaxed structure is typically the result of more complicated deformation modes or strain path changes such as equal channel angular extrusion (ECAE) routes involving sample rotation between passes [10], multiple directional forging [11] and surface mechanical attrition [12]. The structural morphology is also affected by the deformation conditions (e.g. strain, strain rate and temperature) and material parameters (e.g. stacking fault energy, impurity level and the presence of second phase particles).

In the case where an elongated structure is formed, a proper selection of the sample plane is critical to properly reveal the elongated morphology. For example, it has been well demonstrated [7, 13] that in highly strained cold rolled samples a lamellar structure with the lamellar boundaries approximately parallel to the rolling plane develops and that this lamellar structure can be clearly revealed in the longitudinal plane (containing the rolling direction and the normal direction) of the rolled sample. In some early studies of the microstructures developed in ARB processed metals, TEM observations were made in the rolling plane and an equiaxed structure was reported [14]. However, recent more extensive TEM and EBSD characterizations in the longitudinal plane [15–17] have shown the formation of a lamellar structure similar to that observed in conventional cold rolling. Figure 1 shows an example of the lamellar structure revealed by TEM (a) and EBSD (b) in a commercial purity Al after 6 cycle ARB processing.

The microstructures in HPT processed samples have been characterized by many researchers only in the torsion plane [18–20], probably due to the difficulty in preparing TEM foil samples from the longitudinal plane (see Fig. 2) of the small disc samples (typically with a thickness of 1 mm and a diameter of 10 mm) processed by HPT. The morphology observed in the torsion plane is in general described as equiaxed, similar to the early rolling plane observations in cold rolled or ARB processed metals. A similar observation in the torsion plane of an HPT Ni is shown in Fig. 3. It is seen that the morphology is in fact rather complicated although areas with light or dark contrast and irregular shapes can be identified. However, in the longitudinal plane, a well-defined lamellar structure was observed, and an example is shown in Fig. 4a. As schematically shown in Fig. 4b, the lamellar structure is delineated by the lamellar boundaries approximately parallel to the torsion plane. Within the lamellae short boundaries interconnecting the lamellar boundaries are formed. This lamellar structure is similar to that observed after high strain rolling [7, 13] or ARB processing [15, 17]. Note that in the HPT samples there is a strain gradient along the disc radius the sample location (defined by the distance, d, from the sample center in Fig. 2) is an important parameter to relate the microstructure to the strain.

At high strains (von Mises strain $\varepsilon_{vm} > 5$), proper sampling section led to identification of occurrence of deformation twinning in the HPT Ni [21]. An example of deformation twins is shown in Fig. 5. It is seen that the deformation twins are well-confined within the narrowly spaced lamellae (<100 nm) and inclined with respect to the lamellar boundaries. This morphological correlation between the deformation twins and the lamellar boundaries can only be revealed in the longitudinal section since the lamellar structure morphology is only manifested in this sample section. More important, this morphological correlation also indicates that deformation twinning occurred after a significant structural refinement had achieved (<100 nm), in agreement with the suggestion that the deformation twinning is a characteristic deformation mechanism of nanostructured metals [22, 23]. The width of the deformation twins observed varied in a range from a few nanometres to about 30 nm, which is much smaller than the width of pre-existing annealing twins (often sub-micrometer to tens of micrometers) in the undeformed Ni. The misorientation angles measured in terms of Kikuchi diffraction showed a nearly perfect twin misorientation ($60^\circ \langle 111 \rangle$) between the matrix and the deformation twins. Note that any pre-existing twins are destroyed after deformation to the strain level at which deformation twinning takes place.

The strength of samples showing the occurrence of deformation twinning was estimated [21] based on the hardness measurement and it was found that the strength is much higher than the critical resolved shear stress for deformation twinning in Ni. The high pressure applied during the processing may also have an effect on the deformation twinning as similar phenomenon is not easily detected e.g. in tensile straining condition.

In summary, the characteristic structure developed during ARB and HPT is a lamellar structure with the lamellar boundaries parallel to the rolling plane in ARB and parallel to the torsion plane in HPT. This structural

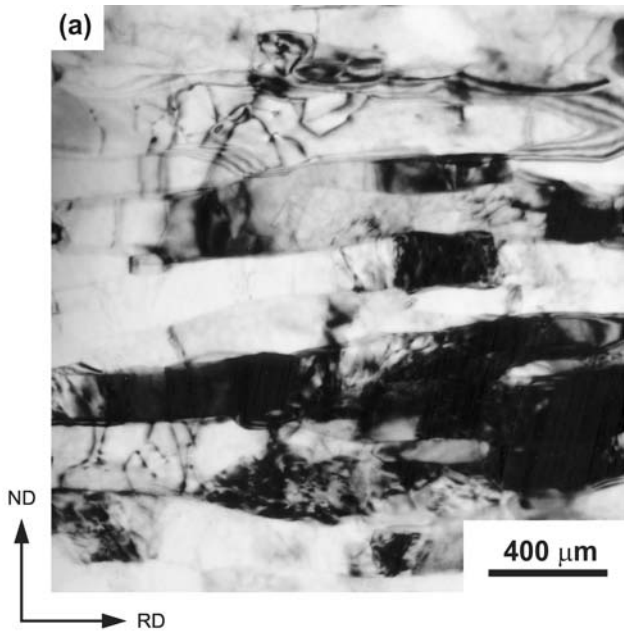

Fig. 1 (**a**) TEM image and (**b**) EBSD boundary map showing the formation of a lamellar structure in a commercial purity aluminum processed by 6 cycle ARB at room temperature

morphology cannot be revealed in the rolling plane or torsion plane but it can be seen in the longitudinal plane, indicating a strong effect of the sampling plane on the identification of the dominating structural features.

Boundary spacing

During plastic deformation, the mean boundary spacing decreases with increasing strain due to grain

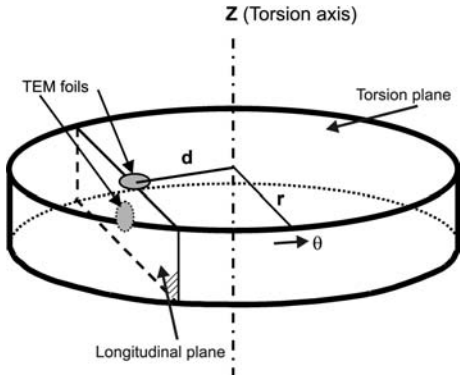

Fig. 2 Schematic drawing of the HPT sample and the sample panes for TEM observations. *Z*: torsion axis. *r*: radius, θ: shear direction. TEM foils are prepared from both the torsion plane and the longitudinal plane (as indicated in the figure) at a distance of d from the disc center, and therefore the plastic strain is well defined

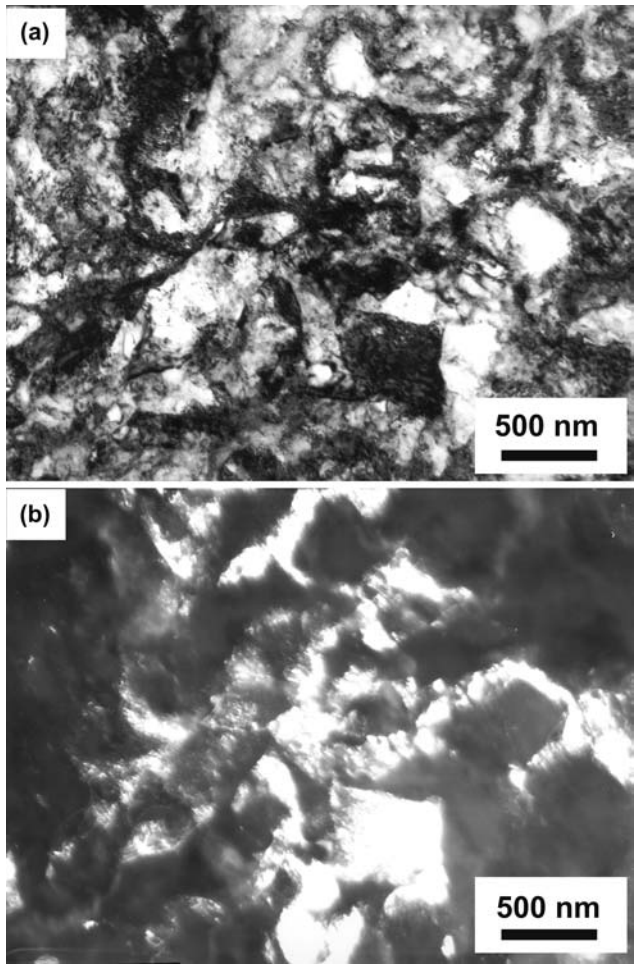

Fig. 3 (**a**) Bright field and (**b**) dark field TEM images showing the structural morphology in the torsion plane of a pure Ni HPT processed to a von Mises strain of about 5. The HPT was carried out under a hydrostatic pressure of 4 GPa

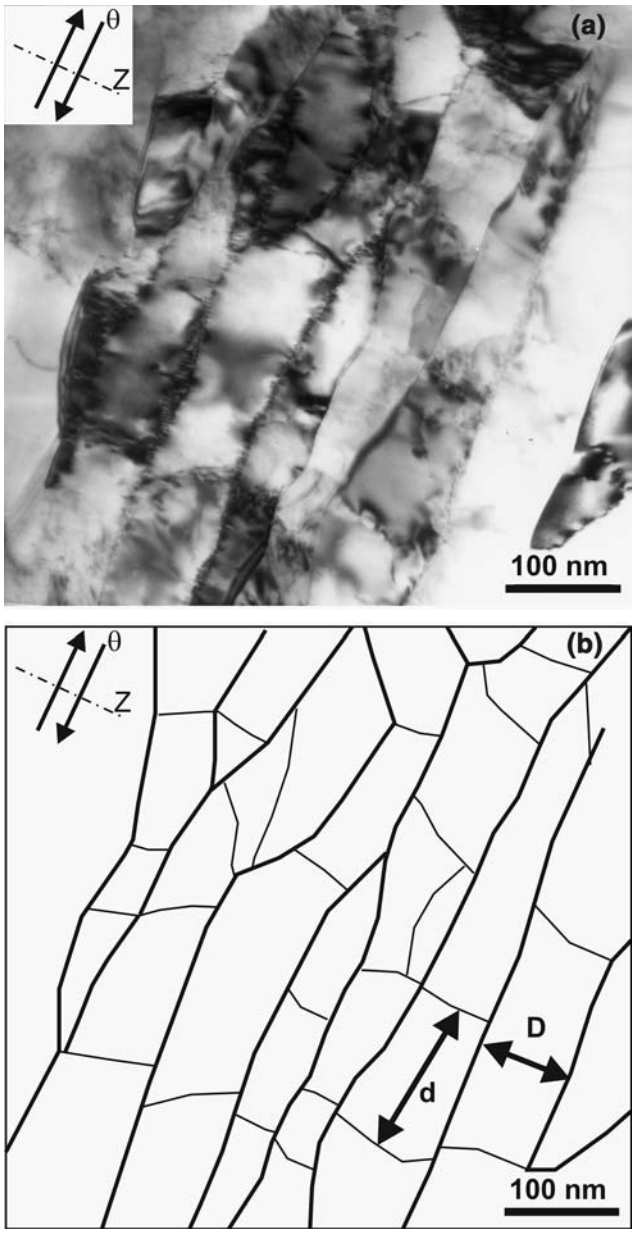

Fig. 4 (**a**) TEM image observed in the longitudinal plane of HPT Ni showing the development of a lamellar structure with the lamellar boundaries approximately parallel to the torsion plane (perpendicular to the torsion axis *Z*). Interconnecting boundaries are formed between the lamellar boundaries. (**b**) A sketch of the lamellar structure seen in (**a**). The boundary spacings for the lamellar boundaries *D* and interconnecting boundaries d are measured, respectively, in the torsion axis direction and the shear direction

subdivision. The boundary spacing in deformation produced nanostructures is typically in the range from a few hundred nanometres to about 100 nm. At very large strains, the boundary spacing can be reduced to about 10 nm [24, 25].

To measure the boundary spacing on transmission electron micrographs, it is necessary to clearly reveal

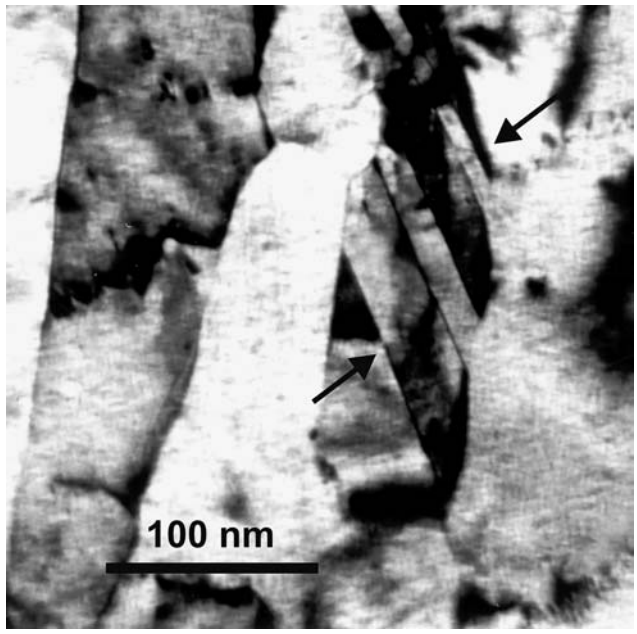

Fig. 5 Deformation twins observed in a pure Ni HPT processed to a von Mises strain of 12. The twins, indicated by arrows, are well confined within a lamella and have widths from nm 8 to 30 nm

the structural morphology. For the lamellar structure, as shown in Fig. 4b, there are two boundary spacings, namely the spacing between the lamellar boundaries (*D*) and the spacing between the interconnecting boundaries (*d*). The mean spacings measured at two strains, $\varepsilon_{vm} = 12$ and $\varepsilon_{vm} = 33$ are given in Table 2. In the literature, the grain size measured from the torsion plane of HPT Ni deformed under various hydrostatic pressures (3–9 GPa) and strains ($\varepsilon_{vm} > 5$) varies in a range of 100–200 nm [19, 20]. These values are comparable with the spacing of interconnecting boundaries measured in the longitudinal plane but significantly larger than the lamellar boundary spacing.

The boundary spacing may also be measured from EBSD orientation image maps or boundary maps when the structural size is larger than the EBSD spatial resolution which is typically above 50–100 nm. However, due to the problem of limited angular resolution, which will be discussed in the next section, low angle boundaries (typically less than 2°) cannot be revealed in the EBSD maps. Therefore, the boundary spacing measured from the EBSD maps is larger than the value measured from the TEM images. When the grain size is smaller than 50–100 nm, the spacing can only measured by TEM and HRTEM methods or by the XRD method. However, it should be noted as mentioned before that the grain size distribution may have a

Table 2 Lamellar boundary spacing (D) and interconnecting boundary spacing (d) measured in HPT Ni deformed to two strains

Strain, ε_{vm}	D	d	Aspect ratio
12	75	200	2.7
33	60	150	2.5

Table 3 Angular and spatial resolution typically available for three electron diffraction based techniques for misorientation measurement

Technique	Angular resolution	Spatial resolution
SAD	>2°	Several hundred nm
Kikuchi diffraction	~0.2°	A few nm
EBSD	~1°	>50 nm

strong effect on the grain size measured by the XRD analysis [5].

Boundary misorientation

During plastic deformation, the mean boundary misorientation increases with increasing strain due to a continuous increase in the fraction of high angle boundaries that are formed by the transformation of low angle dislocation boundaries into high angle boundaries and by the generation of boundaries separating different texture components [26]. Several electron diffraction-based techniques, namely selected area electron diffraction (SAD) and convergent beam Kikuchi electron diffraction in a TEM and EBSD in a SEM, have been extensively used to characterize the misorientation in deformation-produced nanostructures. These techniques have different angular resolutions and spatial resolutions (see Table 3), and caution is required when interpreting the measured results or when using the data for further modeling purposes. In the following, these techniques are reviewed, and issues that may cause misinterpretation of results obtained are discussed.

SAD is an easy method and its spatial resolution depends on the size of the smallest selected area aperture available in a microscope, which is in general larger than several hundred nanometres. When the grain size is larger than this selected area, the misorientation between two grains can be estimated from two SAD patterns obtained from the two grains. However, the angular resolution is in general not better than 2°. For deformation-produced nanostructures, the grain size is generally smaller than the diameter of the smallest selected area aperture. Therefore, many grains may be contained in the selected area, and as a result, a multiple SAD pattern or a ring-like SAD pattern is obtained, as often reported in the literature. In fact, the formation of a ring-like pattern has often been used as evidence of the generation of high angle boundaries in nanostructures. However, an SAD pattern provides only qualitative information on the spread of orientations present in the selected area but not any information on the spatial distribution of these orientations. In other words, although grains of many different orientations can produce a ring-like SAD pattern, the formation of such a pattern does not necessarily indicate the presence of high angle boundaries in the structure. For example, a smooth and continuous lattice curvature over a large angular range can also produce a similar ring-like pattern. In a deformed structure, it is likely that a continuous lattice curvature or an accumulative misorientation is formed over a distance of several hundred nanometres. Therefore, the formation of a ring-like SAD pattern does not provide conclusive information about the development of high angle boundaries.

EBSD is a fully commercialized and automated method. It is a powerful technique to map orientation and misorientation over rather large areas (for example up to the scale of mm^2) and to obtain the misorientation distribution. However, as shown in Table 3, this technique suffers from problems in both the angular resolution and the spatial resolution. The angular resolution depends on the diffraction pattern quality that is affected by many factors such as the quality of the polished sample surface for the EBSD measurements and the dislocation content in the area analyzed. For samples deformed to large strains, the angular resolution is in general not better than 2°. Figure 6a shows an example of misorientation distributions obtained by EBSD for a high purity (99.99%) Al processed by ARB to 6 cycles ($\varepsilon_{vm} = 4.8$) [27]. A very high fraction of high angle boundaries (>15°), >70%, is measured. However, it should be noted that in this distribution the misorientation angles below 2° are not included due to the uncertainty in the misorientation determination. Therefore, the fraction of high angle boundaries obtained by EBSD is overestimated. Such overestimate should be born in mind when relating the measured misorientation to the mechanical and thermal behavior of nanostructured metals. Finally, the relatively large spatial resolution (typically >50 nm) limits the application of the EBSD technique to the characterization of the misorientation in nanostructured metals when the grain size is below the EBSD spatial resolution.

The TEM Kikuchi diffraction method has advantages in both angular and spatial resolution, and thus is

an ideal tool to study misorientations in nanostructured metals. However, the analysis of Kikuchi patterns is still manually based in many laboratories and it is thus a time-consuming process. In our laboratory, a semi-automatic Kikuchi pattern analysis method has been developed [28] and applied to measure boundary misorientations in several nanostructured metals [7, 15, 27]. One example of the results obtained is shown [27] in Fig. 6b from the same sample as was used for EBSD analysis (Fig. 6a) for comparison. It is seen that both EBSD and TEM measurements demonstrate a bimodal distribution with one peak located in the lower end of the misorientation angles and the other located in the upper end. Similar distributions have also been obtained in other nanostructured metals [7, 13, 29], indicating that the bimodal misorientation distribution is a characteristic feature of nanostructured metals. However, as shown in Fig. 6b, about 17% of the boundaries have misorientation angles less than 2°, which are not detected by EBSD (Fig. 6a). This result indicates that to achieve a complete characterization of the misorientation distribution the EBSD technique is not appropriate but that the use of the TEM Kikuchi diffraction technique is required. It should also be noted that the concentration of low angle boundaries with misorientations of less than a few degrees is rather high even for the high purity Al studied (Fig. 6b). The quantification of these low angle boundaries is crucial to establish the correlation between the structural parameters and the mechanical properties of the deformation-produced nanostructures as it has been suggested that the low angle boundaries contribute to dislocation strengthening [30]. However, it should be pointed out that most of the TEM analyses of misorientation distributions have been made for a structure coarser than 100–200 nm. More measurements in finer structures (<100 nm) are required to prove the presence and evolution of low angle dislocation boundaries when the structure is refined down to a scale smaller than 100 nm.

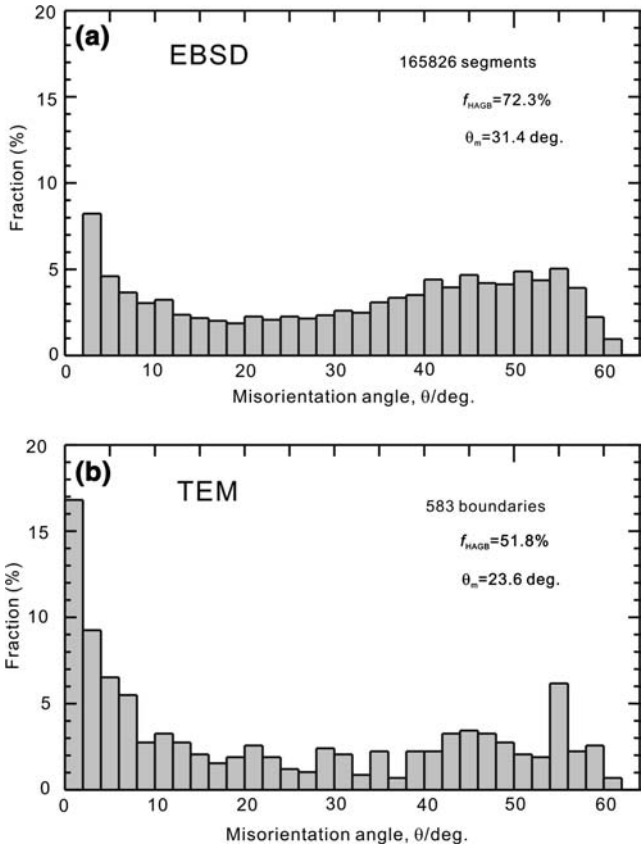

Fig. 6 Misorientation distribution obtained by EBSD (**a**) and TEM (**b**) methods in a high purity aluminum processed by six-cycle ARB. Note the absence of misorientation angles <2° in the first distribution

In summary, due to the different angular and spatial resolutions associated with different electron diffraction techniques, careful selection of the technique is required depending on the purpose and care is required to interpret the results. Moreover, these techniques have different efficiencies in their data acquisition, which also is an issue when selecting a technique. The boundary misorientation angles in the deformation-produced nanostructures exhibit a characteristic bimodal distribution with one peak located in the lower end of misorientation angles and the other located in the upper end. This bimodal distribution clearly illustrates a difference between the boundaries characterizing the deformation-produced nanostructures and those present in a recrystallized structure.

Interior dislocation density

As a product of high strain deformation, the deformation-produced nanostructures always contain a certain amount of interior dislocations and the dislocation density varies depending on which metal and the processing conditions. The existence of interior dislocations may play a key role in determining the mechanical behavior of nanostructured metals [31]. HRTEM and TEM techniques can be used to determine the density of dislocations and their spatial distribution in the structure. The determination of dislocation density by HRTEM relies on the identification of individual dislocations on HRTEM images. Special care is required to avoid the misidentification of Moiré effect-induced lattice image shifting as dislocations, which has been discussed in detail by Rentenberger et al. [6]. In the TEM method, the crucial

issues are the precise determination of the foil thickness and the complete manifestation of all the dislocations present in the structure. Convergent beam diffraction can be used to precisely determine the foil thickness and the multiple beam diffraction is required to reveal the dislocations. Another issue is the possible escape of dislocations to the specimen surface during sample electropolishing [32]. However, it is likely that dislocations escape in nanostructured metals may be less of an issue than in metals with a coarse grain size.

Concluding remarks

The fine scale microstructure in nanostructured metals makes it difficult to quantify the structural parameters. Microstructural characterization techniques such as TEM and EBSD have to be applied to allow the determination of structural parameters as boundary spacing and misorientation angle and distribution of these parameters. Also a quantification of the interior dislocations is a requirement. In this work a careful selection of sample section is suggested. Such careful analysis is a must in the further process development and in order to model the crucial relationship between microstructure and properties in nanostructured metals both in the deformed and in the annealed state.

Acknowledgement The author gratefully acknowledges the Danish National Research Foundation for supporting the Center for Fundamental Research: Metal Structures in Four Dimensions, within which this work was performed. The author also thanks Niels Hansen for helpful discussions and Brian Ralph for critical reading of the manuscript and many good comments.

References

1. Valiev RZ, Islamgaliev RK, Alexandrov IV (2000) Prog Mat Sci 45:103
2. Zhu YT, Langdon TG, Horita Z, Zehetbauer M, Semiatin SL, Lowe TC (eds) (2006) Ultrafine grained materials IV. Warrendale, PA, TMS
3. Erb U, Palumbo G, Szpunar B, Aust KT (1997) Nanostruct Mater 9:261
4. Groza JR (1999) In: Suryanarayana C (ed) Non-equilibrium processing of materials. Oxford, Pergamon UK, p 345
5. Mitra R, Ungar T, Weertman JR (2005) Trans Indian Met 58:1125
6. Rentenberger C, Waitz T, Karnthaler HP (2004) Scripta Mater 51:789
7. Liu Q, Huang X, Lloyd DJ, Hansen N (2002) Acta Mater 53:3789
8. Tsuji N, Saito Y, Lee SH, Minamino Y (2003) Adv Eng Mater 5:338
9. Huang X, Vorhauer A, Winther G, Hansen N, Pippan R, Zehetbauer M (2004) In: Zhu YT, Landon TG, Valiev RZ, Shin DH, Lowe TC (eds) Ultrafine grained materials III. TMS, p 235
10. Furukawa M, Horita Z, Langdon TG (2002) Mater Sci Eng A 332:97
11. Sitdikov O, Sakai T, Goloborodko A, Miura H, Kaibyshev R (2005) Phil Mag 85:1159
12. Zhang HW, Hei ZK, Liu G, Lu J, Lu K (2003) Acta Mater 51:1871
13. Hughes DA, Hansen N (2000) Acta Mater 48:2985
14. Saito Y, Tsuji N, Utsunomiya H, Sakau T, Hong RG (1998) Scripta Mater 39:1221
15. Huang X, Tsuji N, Hansen N, Minamino Y (2003) Mater Sci Eng A340:265
16. Tsuji N, Saimoto Y, Lee SH, Minamino Y (2003) Adv Eng Mater 5:338
17. Li BL, Tsuji N, Kamikawa N (2006) Mater Sci Eng A 423:331
18. Valiev RZ, Ivanisenko YV, Rauch EF, Baudelet B (1996) Acta Mater 44:4705
19. Zhilyaev AP, Nurislamova GV, Kim B-K, Baró MD, Szpunar JA, Langdon TG (2003) Acta Mater 51:753
20. Dalla Torre F, Spätig P, Schäublin R, Victoria M (2005) Acta Mater 53:2337
21. Huang X, Winther G, Hansen N, Hebesberger T, Vorhauer A, Pippan R, Zehetbauer M (2003) Mater Sci Forum 426–432:2819
22. Zhu YT, Liao XZ, Srinivasan SG, Zhao YH, Baskes MI, Zhou F, Lavernia EJ (2004) Appl Phy Lett 85:5049
23. Froseth AG, Derlet PM, Van Swygenhoven H (2005) Adv Eng Mater 7:16
24. Hughes DA, Hansen N (2001) Phys Rev Lett 87:135503.1
25. Zhang HW, Hansen N (this issue)
26. Hughes DA, Hansen N (1997) Acta Mater 45:3871
27. Kamikawa N, Tsuji N, Huang X, Hansen N (2007) Acta Mater (in press)
28. Liu Q (1995) Ultrmicroscopy 60:81
29. Huang X, Kamikawa N, Hansen N (2006) Mater Sci Eng
30. Hansen N (2004) Scripta Mater 51:801
31. Huang X, Hansen N, Tsuji N (2006) Science 312:249
32. Foxon CTB, Rider JG (1968) Phil Mag 17:729